Available online at www.sciencedirect.com
ScienceDirect
Thin Solid Films 516 (2007) 422–427
www.elsevier.com/locate/tsf

Corrosion behavior of AZ91 magnesium alloy treated by plasma immersion ion implantation and deposition in artificial physiological fluids

Chenglong Liu [a], Yunchang Xin [a,b], Xiubo Tian [a,c], Paul K. Chu [a,*]

[a] Department of Physics and Materials Science, City University of Hong Kong, Tat Chee Avenue, Kowloon, Hong Kong, China
[b] Tsinghua University, Shenzhen Graduate School, Shenzhen 518055, China
[c] State Key Laboratory of Welding Production Technology, School of Materials Science and Engineering, Harbin Institute of Technology, 15001, China

Available online 2 June 2007

Abstract

Due to the good biocompatibility and tensile yield strength, magnesium alloys are promising in degradable prosthetic implants. The objective of this study is to investigate the corrosion behavior of surgical AZ91 magnesium alloy treated by aluminum, zirconium, and titanium plasma immersion ion implantation and deposition (PIII&D) at 10 kV in artificial physiological fluids. The surface layers show a characteristic intermixed layer and the outer surface are mainly composed of aluminum, zirconium or titanium oxide with a lesser amount of magnesium oxide. Comparing the three sets of samples, aluminum PIII&D significantly shifts the open circuit potential (OCP) to a more positive potential and improves the corrosion resistance at OCP.

PACS: 87.68.+z Biomaterials; 52.77.Dq Plasma-based ion implantation and deposition; 81.65.Kn Corrosion protection
Keywords: Magnesium alloy; Plasma immersion ion implantation and deposition; Corrosion; Physiological fluid

1. Introduction

Magnesium alloys were first introduced into orthopedic and trauma surgery in the first half of the last century [1]. Compared to current implant materials such as Ti and titanium alloy, stainless steel and CoCr alloy, AZ91 magnesium alloys provide a lower elastic modulus (45 GPa) and higher tensile yield strength (200 MPa) [2]. However, the poor corrosion in physiological fluids has hampered widespread use in prosthetic devices. Although the development of casting technique has improved the corrosion resistance of magnesium alloys, the associated process is quite complex and costly. Plasma immersion ion implantation and deposition (PIII&D) is one of the effective ways to synthesize an intermixed structure in the near-surface of materials for improved surface properties [3–5]. Some studies on metal or non-metal ion implantation with magnesium or magnesium alloy have recently been performed. Ion implantation of metal ions such as Cr [5], Al [6], Ta [7] can form a new oxidized film on the surface as well as an intermixed layer composed of the metallic compound resulting in enhanced corrosion resistance in different media. The effects of N^+, H^+, and H_2O implantation on the corrosion behavior of magnesium alloy have been studied. The more compactness surface oxide layer in conjunction with N^+ or H_2O implantation gives rise to higher corrosion resistance [8,9]. At the same time, formation of MgH_2 enhances the corrosion resistance of H-implanted high purity magnesium or AZ91 magnesium alloys [10]. These studies were conducted for industrial applications and the biological effects have not been extensively investigates. There have been few reports on the corrosion behavior of AZ91 Mg alloy after surface modification by metal plasma immersion ion implantation and deposition (PIII&D) in simulated body fluids. In this work, we investigate the effects of different PIII&D on the corrosion behavior of AZ91 magnesium in simulated body fluids.

2. Experimental details

Commercially available extruded AZ91 alloys with dimensions of 10 mm × 10 mm × 2 mm were prepared. The specimens were ground with water-proof SiC paper No. 400, 1200 and

* Corresponding author. Tel.: +852 27887724; fax: +852 27889549.
E-mail address: paul.chu@cityu.edu.hk (P.K. Chu).

0040-6090/$ - see front matter © 2007 Elsevier B.V. All rights reserved.
doi:10.1016/j.tsf.2007.05.048

2400 grits sequentially and then ultrasonically washed in ethanol for 10 min. In the aluminum, zirconium and titanium PIII&D experiments, a metal vapor vacuum arc source was used and a pulsed high voltage of −10 kV was applied to the specimens. During the high-voltage off-cycles, deposition of metal particles occurred and ion implantation was conducted during the on-cycles. Implantation and deposition thus proceeded alternately and the PIII&D time was 4 h.

The surface composition and depth profiles were obtained by X-ray photoelectron spectroscopy (XPS, PHI 5802) by means of argon sputtering using a monochromatic Al K_α radiation. High-resolution XPS spectra were taken at different sputtered depths to investigate the chemical states of the implanted species. The corrosion and electrochemical behavior of the as-received and PIII&D specimens were studied in Hank's simulated body fluid (SBF) at 37±1 °C. The open circuit potential (OCP) tests were conducted on an EG&G 263A potentiostat/galvanostat. Changes in the OCP were recorded as a function of time during an exposure time of about 4000 s. The electrochemical impedance spectroscopy (EIS) measurements were carried out on the GAMRY PCI4/300 at a stable OCP. The perturbing signal had an AC amplitude of 10 mV and frequency range from 100 kHz to 10 mHz. The data were analyzed through the software Gamry Echem Analyst.

3. Results and discussion

AZ91 alloy is mainly composed of Mg, Al, and Zn. XPS measurements were carried out to determine the elemental concentration in the modified layer as a function of depth. Fig. 1 depicts the XPS depth profiles acquired from the Ti-PIII&D AZ91 alloys. Fig. 1(a) shows a roughly Gaussian Ti depth distribution in the Ti-PIII&D sample. The peak concentration is approximately 52 at.% at a depth of ~28 nm. At depths exceeding 40 nm, the Mg and Al concentrations increase gradually. Fig. 1(b) depicts the changes in the Mg, Ti, Al, and O valence states with depths. At the near-surface region, the Mg 1s peak at 1302.7 eV corresponds to $Mg(OH)_2$. At a depth of about 40 nm, the peak at 1304.0 eV indicates the existence of $MgAl_2O_4$ and at 56 nm, the peaks at 1303.1 eV and 1304.0 eV correspond to metallic Mg. Based on the Ti 2p patterns in Fig. 2(a), the surface is composed partially of titanium oxide as indicated by the two

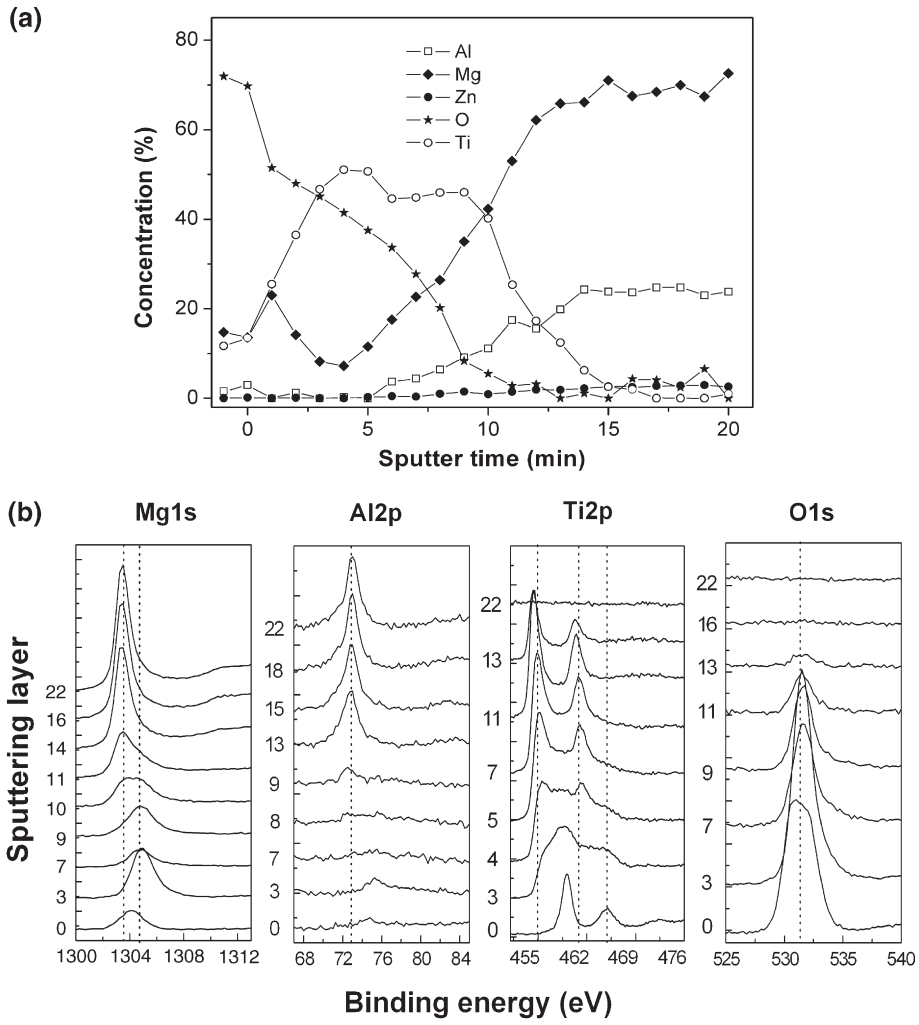

Fig. 1. (a) XPS depth profiles obtained from the magnesium alloy after Ti PIII&D at 10 kV (sputtering rate=5.6 nm/min). (b) High-resolution XPS spectra of Mg1s, Al2p, Ti2p and O1s obtained from the Ti-PIII&D magnesium alloy.

peaks at 458.7 (2p3/2) eV and 464.5 (2p1/2) eV. At depths exceeding 50 nm, peaks at 454.2 (2p3/2) and 460.3 (2p1/2) arise from metallic Ti [11]. The alloy component Al is seen to exist mainly as oxide on the surface and as metallic Al in the subsurface as shown in Fig. 1(b). At depths up to 40 nm, the Al 2p peak at 74.7 eV corresponds to Al_2O_3 and between 40 nm and 60 nm, the peaks at 74.3 eV and 72.8 eV coexist, implying the existence of Al_2O_3 and metallic Al. At depths over 60 nm, the single peak at 72.9 eV corresponds to metallic Al [11]. The relatively wide O 1s peak shifts from 529 eV to 534 eV at the near-surface. It is almost asymmetric and can be deconvoluted into peaks corresponding to the O^{2-} state such as Al_2O_3 (531.1 eV, alpha 531.8 eV, gamma 530.9 eV), MgO (530.0 eV, 531.2 eV, 532.1 eV) and TiO_2 (529.9 eV) and one at ~31.4 eV corresponding to OH^- species. At depths exceeding 60 nm, the O 1s peak becomes weaker [11]. The O 1s spectra confirm the compositional structure indicated by the other elements. Based on the XPS results, the tri-layer structure in the Ti-PIII&D AZ91 alloy has the following compositions. The outer layer, about 10 nm thick, is mainly composed of MgO and TiO_2 with less $Mg(OH)_2$. The middle layer that is 50 nm thick comprises predominantly TiO_2 and MgO with minor contributions from $MgAl_2O_4$ and TiO. The third layer is rich in metallic Mg, Ti, Al and Ti_3Al. No abrupt boundaries among these layers are observed due to ion mixing.

The depth profiles of the Al-PIII&D samples are shown in Fig. 2(a). At a depth of about 10 nm, the Mg concentration is approximately 5 at.%. An intermixed surface layer consisted of mainly aluminum oxide is formed. From 10 nm to 70 nm, the aluminum concentration is relatively constant but the magnesium concentration increases quickly. At depths over 70 nm, the Al concentration decreases gradually. The maximum Al concentration is about 35 at.%. The results corroborate the formation of a triple-layer structure. Fig. 2(b) displays the high-resolution XPS spectra of Mg 1s, Al 2p and O 1s taken at different depths. At about 10 nm, Al_2O_3 and $Mg(OH)_2$ are detected. With increasing depths, the amount of metallic aluminum increases as indicated by the increasing intensity of

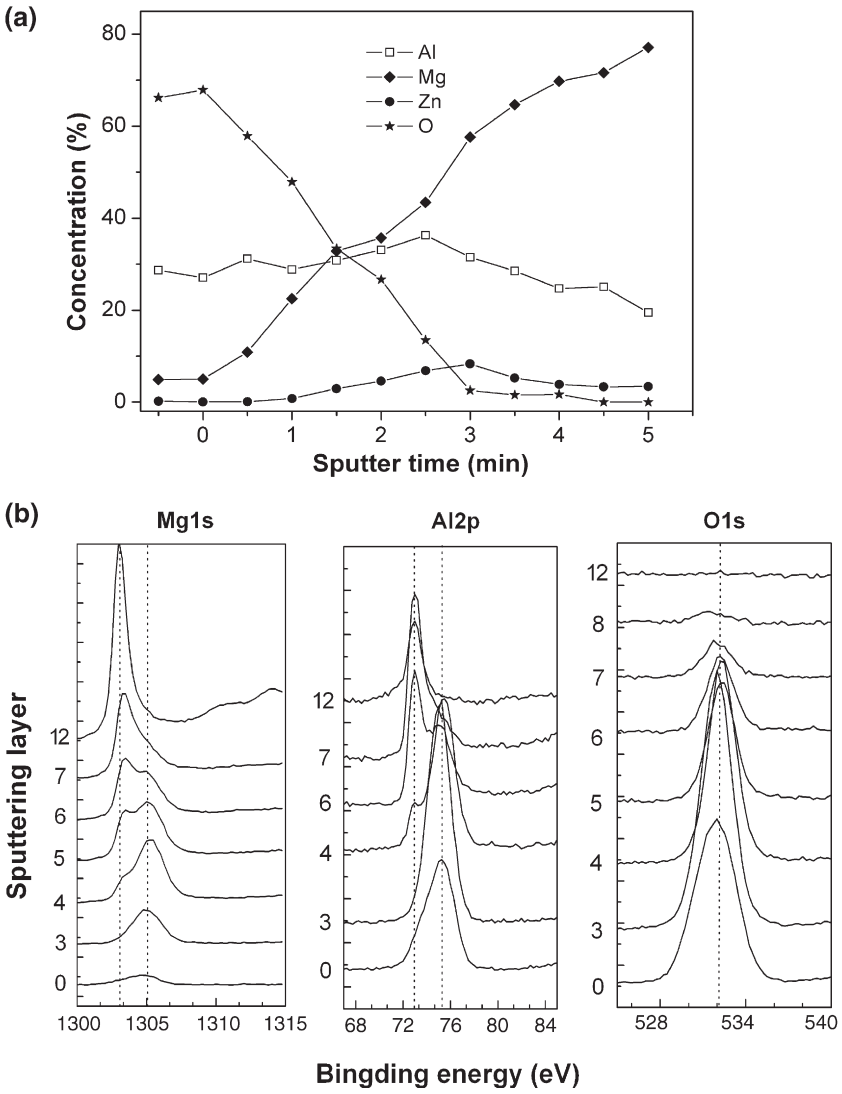

Fig. 2. (a) XPS depth profiles obtained from the magnesium alloy after Al PIII&D at 10 kV (sputtering rate=22.8 nm/min). (b) High-resolution XPS spectra of Mg1s, Al2p and O1s obtained from the Ti-PIII&D magnesium alloy.

an additional plasmon energy loss peak [12] at approximately 72.9 eV. The Al_2O_3 plasmon peak which is at 74.7 eV diminishes in intensity with depths. At a sputter depth of approximately 80 nm, only the peaks corresponding to metallic Al can be detected. In addition, the changes in the Mg valence states are similar to those of the Ti ion implanted samples. Considering the results in Fig. 2(a) and (b), the Al implanted layer is composed of the following microstructure: an outer layer (about 30 nm) consisting of aluminum oxide rich layer with a lesser amount of $Mg(OH)_2$, an intermediate layer rich in magnesium oxide with aluminum and zinc oxide as well as metallic elements, and a bottom layer composed of entirely metallic elements.

The zirconium depth distributions of the Zr-PIII&D sample are shown in Fig. 3(a). The peak concentration of Zr is approximately 67 at.% at a depth of 22 nm. Compared to the Al and Ti-PIII&D samples, the peak concentrations are different. The XPS spectra of the Zr-PIII&D magnesium alloy are shown in Fig. 3(b) taken with increasing depths. The Mg 1s, Al 2p and O 1s XPS spectra are similar to those of the Ti-PIII&D samples. At depths between 0 and 20 nm, zirconium exists in two forms: ZrO_2 (182.4 eV) and Zr (178.9 eV) [11]. At larger depths up to 60 nm, zirconia gradually changes to metallic zirconium. Here, the tri-layer zirconium implanted surface consists of an outer layer rich in zirconia, an intermediate layer composed of zirconium and magnesium oxide as well as metallic zirconium and magnesium, and a bottom layer consisting of the metallic elements.

The aforementioned results show the surface native oxide about 6 nm in thickness [13] is sputtered by during metal ion PIII&D at −10 kV. Under our non-UHV (ultra high vacuum) conditions (about 1.5×10^{-5} Torr) in the PIII&D chamber, surface oxidation is inevitable [15]. In addition, the elevated sample temperature during PIII&D increases the thickness of this surface oxide. Our results indicate that the oxide formed in our process is more compact and may form a better protective layer.

With regard to the electrochemical results, compared to the as-received AZ91 alloy, the Al-PIII&D specimens show the most positive OCP value after 4000 s immersion of about

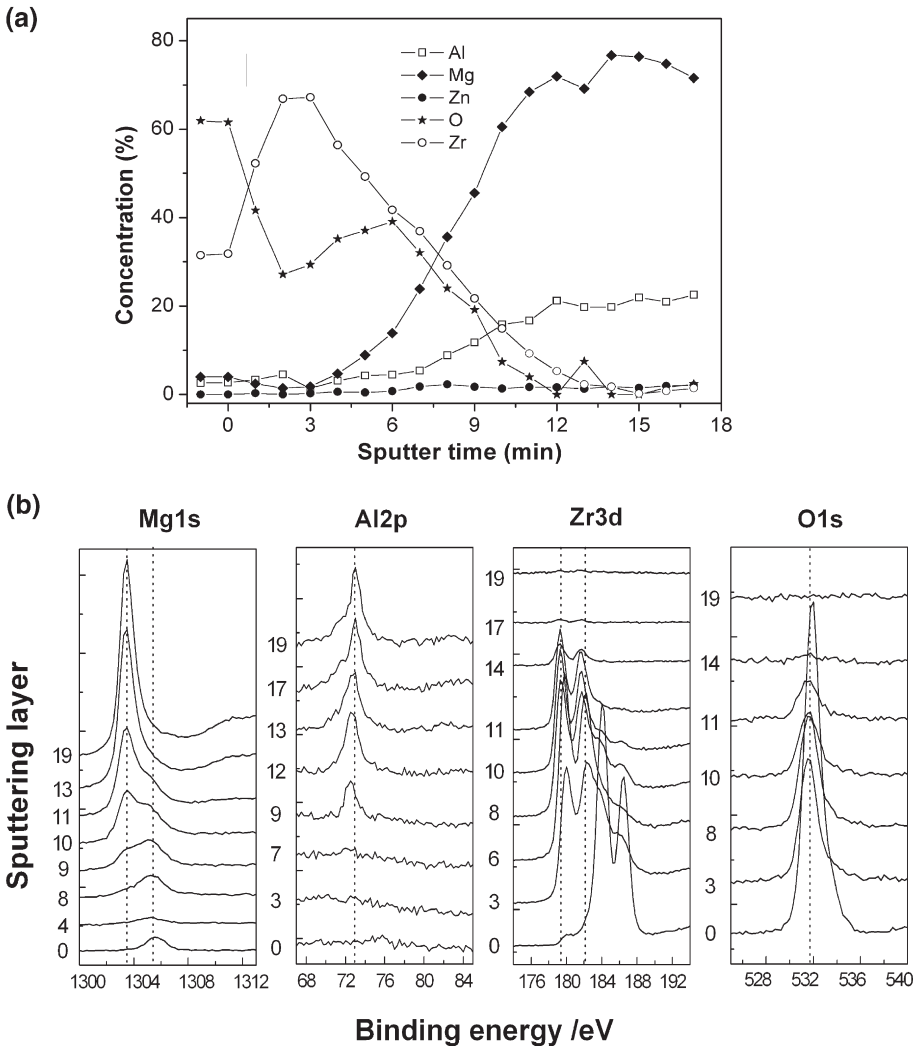

Fig. 3. (a) XPS depth profiles obtained from the magnesium alloy after Zr PIII&D at 10 kV (sputtering rate = 5.6 nm/min). (b) High-resolution XPS spectra of Mg1s, Al2p, Zr3d and O1s obtained from the Zr-PIII&D magnesium alloy.

0.036 V, followed by Zr and Ti-PIII&D specimens at −0.545 V and −0.696 V, respectively. The increase in the OCP values indicates that the electrochemical stability of magnesium alloy can be improved by metal PIII&D, especially aluminum.

Electrochemical impedance spectroscopy (EIS) is one of the most important techniques to investigate the electrochemical behavior of passivation films. Fig. 4 exhibits the Nyquist plots of the EIS spectra of the as-received and PIII&D AZ91 alloys after 4000 s immersion in simulated body fluids. The spectra acquired from AZ91 are characterized by three distinct loops: capacitive in the high frequency range, capacitive in the intermediate frequency range, and inductive in the low frequency range. A closer look reveals differences in the spectra of the modified samples. The two capacitive loops at the high frequency range are fuzzy and an inductive loop in the low frequency range is clear. Here, it is suitable to use an equivalent circuit (EC) ($R_e(Q_fR_f)(Q_{dl}R_t(R_lL))$) to fit the parameters of the corresponding samples. The EC consists of R_e, resistance of the electrode between the working and reference electrodes, a charge transfer resistance, R_t(electron transfer) parallel to the double layer constant phase element (CPE) at the vulnerable regions, Q_{dl}, and a CPE assigned to the layer, Q_f, parallel to the film resistance, R_f. The fitting error here is less than 10% (Table 1).

The observed difference in the Nyquist plots suggests different corrosion processes in the as-received and modified samples. R_f is the relevant resistance for pore or ionic conducting defect resistance [15]. The EIS fits indicate that the Al-PIII&D samples have R_f values about one order of magnitude higher than the as-received samples of approximately 1210 Ω cm^2, followed by zirconium PIII&D. In contrast, titanium PIII&D only has a small influence on the corrosion resistance which is about 441 Ω cm^2 that is about 4 times higher than that of the as-received samples. The difference confirms that the corrosion protection provided by the native oxide film is inferior to that by the implanted and deposited metal particles. In the test solution, the protective oxide layer formed by metal ion PIII&D helps to depress chemical dissolution, electrochemical reactions, and electrolyte penetration. The change in R_f suggests different compactness of the implanted oxide layer. The XPS results show that Al or Zr PIII&D creates an outer layer rich in Al_2O_3 or Z_rO_2, which inhibits oxygen evolution from the implanted surface [7,14]. In contrast, the outer oxide layer on the Ti-PIII&D samples is composed of MgO and $TiO_2$with less $Mg(OH)_2$, and the existence of MgO may decrease the stability of the protective oxide layer [14]. The R_t values reflect the Faradic charge transfer resistance related to electrochemical reactions in the vulnerable regions [15]. The as-received samples have a low R_t value of about 103 Ω cm^2 which is approximately 1/20 of that of the Al-PIII&D samples. This can be ascribed to the difference in the corrosion products at the corrosion pits on the as-received and modified specimens. For the as-received specimens, the fast H_2 evolution velocity mitigates precipitation of $M(OH)_n$ [15], and so the $R_t$value is low. In contrast, it fosters precipitation of the corrosion products due to the lower corrosion rate of the PIII&D specimens thereby enhancing the corrosion protection.

Table 1
EIS fitting results obtained from the as-received and PIII&D AZ91 alloy

Sample	R_e/Ω cm^2	Q_f/10^{-5} F cm^{-2}	R_f/Ω cm^2	Q_{dl}/10^{-5} F cm^{-2}	R_t/Ω cm^2
AZ91	80.02	2.709	93.70	1.612	103.3
Al-PIII&D	69.78	5.508	1210	48.15	2230
Ti-PIII&D	69.73	6.852	442.10	12.82	1154
Zr-PIII&D	69.20	23.71	755.50	60.25	2215

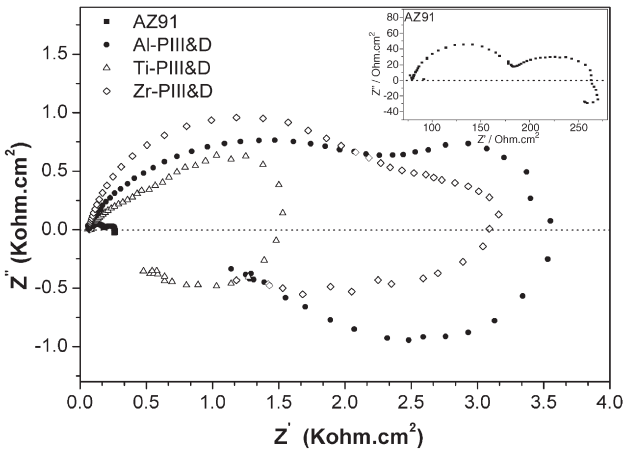

Fig. 4. Nyquist plots of the as-received and PIII&D AZ91 alloy in simulated body fluids after 4000 s immersion.

The micro-corrosion morphologies of the as-received and modified AZ91 alloy after EIS tests show severe corrosion attack on the AZ91 alloy. The corrosion holes which are not uniform arise from the α matrix and β particles [15]. In comparison, less corrosion attack is found on the surface of the Al-PIII&D samples. The corrosion morphologies are consistent with the EIS results. R_f is a parameter reflecting the property of the passivation film. The Al-PIII&D sample has the most positive R_f value, and therefore, it suffers least corrosion attack. In comparison, the lowest R_f value observed from the as-received sample corresponds to the most severe corrosion.

4. Conclusion

Titanium, aluminum and zirconium are plasma-implanted into AZ91 magnesium alloys to improve the corrosion resistance. Metal plasma immersion ion implantation and deposition results in an implanted layer with a tri-layer microstructure with an outer layer composed of mainly metal oxide with a small amount of MgO and $Mg(OH)_2$, an intermediate layer containing metal oxide and metallic implanted particles, and a bottom layer rich in metallic elements. Electrochemical corrosion tests indicate that metal PIII&D can improve the corrosion resistance of the magnesium alloy. Our results show the aluminum implantation and deposition offers the best corrosion protection and the enhancement can be attributed to the compact Al_2O_3 layer and thick intermixed layer.

Acknowledgements

The work is financially supported by City University of Hong Kong Applied Research Grant (ARG) No. 9667011.

References

[1] F. Witte, V. Kaese, H. Haferkamp, H. Windhagen, Biomaterials 26 (2005) 3557.
[2] J.R. Davis, Handbook of Materials for Medical Devices, ASM International, USA, 2003.
[3] J.E. Gray, B. Luan, J. Alloys Compd. 336 (2002) 88.
[4] L. Kutsenko, D. Fuks, A. Kiv, I. Brown, Acta Mater. 16 (2004) 4329.
[5] J. Bruckner, R. Gunzel, E. Richter, W. Moller, Surf. Coat. Technol. 103–104 (1998) 227.
[6] M.K. Lei, P. Li, H.G. Yang, X.M. Zhu, Surf. Coat. Technol. 201 (2007) 5182.
[7] X.M. Wang, X.Q. Zeng, G.S. Wu, S.S. Yao, Mater. Lett. 61 (2007) 968.
[8] X.B. Tian, C.B. Wei, S.Q. Yang, R.K.Y. Fu, P.K. Chu, Surf. Coat. Technol. 198 (2005) 454.
[9] X.B. Tian, C.B. Wei, S.Q. Yang, R.K.Y. Fu, P.K. Chu, Nucl. Instrum. Methods Phys. Res., B Beam Interact. Mater.Atoms 242 (2006) 300.
[10] A. Bakkar, V. Neubert, Corros. Sci. 47 (2005) 1211.
[11] J.F. Moulder, W.F. Stickle, P.E. Sobol, Hankbook of X-ray Photoelectron Spectroscopy, Perkin-Elmer Corporation, USA, 1992.
[12] E. Wieser, I. Tsyganov, Surf. Coat. Technol. 111 (1999) 103.
[13] N. Hara, Y. Kobayashi, D. Kagaya, Corros. Sci. 5 (2006) 33.
[14] Y.Z. Liu, X.T. Zu, C. Li, Corros. Sci. 49 (2007) 1069.
[15] Y.J Zhang, C.W. Yan, F.H. Wang, W.F. Li, Corros. Sci. 47 (2005) 2816.